

High-resolution analysis of Zn²⁺ coordination in the alkaline phosphatase superfamily by EXAFS and x-ray crystallography

Supplemental Material

1. Investigation of a Close Contact Between Ser102 and Phosphate in the *E. coli* Alkaline Phosphatase Structure

Our initial refinement of the wild-type AP structure with inorganic phosphate bound in the active site yielded a very close contact between Ser102 and phosphate. In the four chains of the asymmetric unit, the distance between O γ of Ser102 and the closest phosphate oxygen ranged from 1.64-1.85 Å in refined structures (Figure S1, A-D). These O-O distances are considerably shorter than expected for a hydrogen bond (>2.39 Å) and they approach the distances expected for a covalent O-O (1.48 Å) or O-P (1.56 Å) bond (1-7).

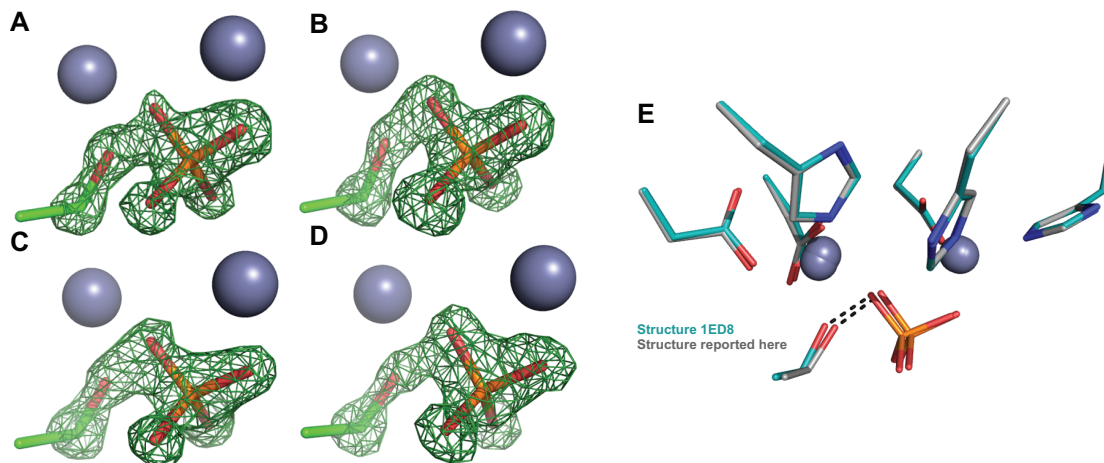


Figure S1. Wild-type AP structures with noncovalently bound inorganic phosphate show close contacts between Ser102-O γ and phosphate. Figures (A)-(D) show F_o-F_c omit maps for chains A-D, respectively, in which the serine side chain and phosphate were deleted from the model before refinement. The maps are contoured at 7σ . (E) Overlay of the 1.29 Å structure reported here with the prior structure 1ED8. Chain A is shown in both structures.

These short distances are also evident in the 1.75 Å wild-type structure 1ED8, deposited by Kantrowitz and coworkers (8) (Figure S1E). Structure 1ED8 has O-O distances of 1.63 Å and 1.43 Å in the two chains of the asymmetric unit. In the published paper associated with structure 1ED8, the short O-O distance was attributed to disorder in the phosphate position (8). However, in the 1.29 Å resolution structure reported here, distinct density was evident for phosphate (Figure S1 A-D), and inorganic phosphate was refined with an average atomic B-factor of 14 Å², similar to the average B-factor of the overall structure of 12 Å², suggesting that disorder of the phosphate cannot fully account for the short distances.

The electrostatic interaction of phosphate with the positive charge of the two zinc ions could provide a driving force to offset the energetically unfavorable close interaction with Ser102, with further implications for catalysis (discussed below). However, it remained possible that the close interaction arises from artifacts of structure determination, and we thus considered additional possible origins for the apparently short O-O distance.

Longer O-O distances are not consistent with the experimental data. To further evaluate whether disorder or ambiguity of the density might contribute to the short O-O distance, we tested whether the crystallographic data were also consistent with a longer distance between Ser102 O γ and the phosphate oxygen. Refinement tests with PHENIX (9) were performed in

which the distance between the close-contacting Ser102 O γ oxygen and phosphate was constrained to 2.2 Å or slightly longer, to 2.4 Å, consistent with a short H-bond (7). Ser102 was allowed to occupy three different conformations (as discussed below) and the occupancies of the three conformations were allowed to vary. Restraining the Ser102-phosphate distance to 2.2 Å in the primary Ser102 conformation ($\chi_1 = -60^\circ$) resulted in both positive and negative difference density in $F_o - F_c$ maps (Figure S2). Restraining the distance to 2.4 Å resulted in substantial difference density. These observations indicate that the density is consistent with an O-O distance of less than 2.2 Å and that disorder, ambiguity, or limitations of the refinement potentials cannot account for the short distance in a straightforward manner.

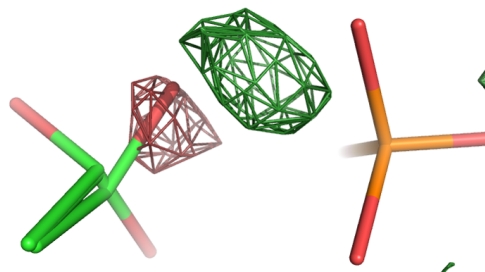


Figure S2. Difference density ($F_o - F_c$) from refinement in which the distance between Ser102-O γ and phosphate was restrained to 2.2 Å. The map was contoured at 3σ , with positive density in green and negative density in red.

Reduced occupancy does not fully account for the short O-O distances. The occupancies of inorganic phosphate refined to 69-76% in the four chains of the submitted structure. Thus, roughly a quarter of the population of molecules could potentially have the Ser102 side chain occupying a conformation that would otherwise clash with the bound phosphate. In addition, the primary conformation of the Ser102 side chain (seen in Figure S1) shows negative density in $F_o - F_c$ maps, suggesting reduced occupancy of this conformation. Reduced occupancy of both Ser and phosphate would correspondingly reduce the occupancy of the species containing the short O-O distance. Thus, we performed refinement tests to obtain a rough estimate of the occupancy of the primary conformation of Ser102.

Kantrowitz and coworkers had previously reported ~40% occupancy of a single alternative conformation of Ser102 in phosphate-bound structure 1ED8 (8). Although well-defined density was not observed for other conformations of Ser102 in the structure reported here, minor positive density was observed, consistent with low or disordered occupancy of alternative conformations. When refinement tests with PHENIX (9) were performed with the occupancy of the Ser102 O γ oxygen allowed to vary, the occupancy of O γ varied from 71-74% in the four chains (Table S1). Refinement of Ser102 with varying occupancy of two or three allowed conformations yielded refined structures with total occupancies of alternative conformations between 22% and 35% (Table S1).

Disorder or possible alternative conformations of Ser102 would reduce the population of the serine side chain that appears to closely contact the phosphate oxygen. However, even partial occupancy of both phosphate and the Ser102 ($\chi_1 = -60^\circ$) could not fully account for the close O-O distance in the model. If, for example, the occupancies of phosphate and Ser102 ($\chi_1 = -60^\circ$)

were both 70%, a minimum of 40% occupancy remains for the species in which Ser102 and phosphate occupy very close positions.

Table S1. Refinement with alternative conformations of Ser102^a

Experiment	Chain	Occupancy for conformations of Ser102, %		
		$\chi 1 = -60^\circ$	$\chi 1 = 180^\circ$	$\chi 1 = +60^\circ$
Refinement with occupancy of Ser102 O γ floated	A	72		
	B	71		
	C	74		
	D	71		
Refinement of Ser102 occupancy split between two conformations	A	78	22	
	B	76	24	
	C	77	23	
	D	76	24	
Refinement of Ser102 occupancy split among three conformations	A	69	20	11
	B	65	18	17
	C	67	19	14
	D	67	19	13
Structure 1ED8	A	58	42	
	B	57	43	

^a Refinement tests were performed with PHENIX. Phosphate was not modeled in these tests.

Including covalent phosphoserine does not account for the short O-O distance. Another potential origin of a short O-O distance is a contribution to the observed electron density from a covalent enzyme-phosphate species. In other words, a small fraction of the enzyme could exist in a state where serine is covalently linked to the phosphorus atom (Ser-O-PO₃²⁻), a state that represents an intermediate along the enzymatic reaction pathway. The clear density for four separate oxygen atoms indicates that covalent phosphoserine would be a minor species, if present (Figures S1 and S3). Refinement tests in which covalent phosphoserine was included with varied, fixed occupancies showed very little change in difference density between 0% and 20% covalent species, suggesting that up to 20% phosphoserine could be present without altering the electron density.

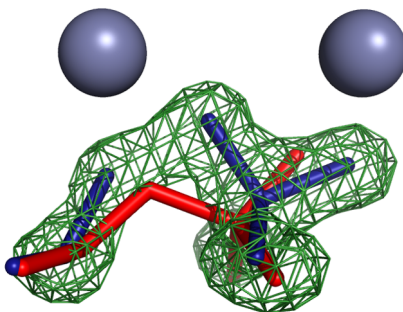


Figure S3. Covalent phosphoserine (red, Ser-O-PO₃²⁻) is modeled and shown with noncovalently bound phosphate (blue). An omit map from Figure S1 is shown in green, illustrating that the noncovalently bound species predominates. However, refinement tests with between 0% and 20% covalent phosphoserine showed very little change in difference density.

However, based on measurements of individual rate and equilibrium constants for phosphorylation and dephosphorylation of AP with inorganic phosphate, the equilibrium constant for the interconversion of covalent and noncovalent species is 99 ± 17 and thus the expected fraction of covalent phosphoenzyme species is around 1% at pH 7 and 0 °C (10). The fraction of covalent phosphoenzyme is expected to be even lower in the crystallization buffer at pH 8. While it is possible that a greater than expected fraction of covalent species exists because of the uncertainty of the pH and conditions of the crystallization solution after 6 months of vapor diffusion, the simplest expectation is that 1% or less of the phosphate is bound in the covalent phosphoserine form. Even if the maximum of 20% of the phosphate occupancy existed in the covalent form, this would not be sufficient to explain the close O-O distance, because the majority of the phosphate remains in the noncovalent form.

Implications of a short O-O distance. The observations reported above suggest that the Ser102 side chain and phosphate occupy positions that produce a close O-O contact ($< 2.2 \text{ \AA}$) some proportion of the time, estimated to be 40% or more. Some precedent exists for short O-O distances in currently available structures. A search of the 2010 edition of the small-molecule Cambridge Structural Database (11) revealed around 200 structures with C-O...O-C or P-O...O-C distances of 1.5-2.1 Å. As of June 2011, the Protein Data Bank contained 7 protein contacts with O-O distances of 1.5-2.1 Å that also met the following criteria: resolution better than 1.3 Å, B-factors less than 30 \AA^2 , occupancies of 1, and no direct covalent linkage. However, inspection of electron density of these structures suggested that some of these short contacts may arise from ambiguity or disorder of the density.

The observed short O-O distance in AP would likely represent a repulsive interaction, because it is too short to form a favorable hydrogen-bonding geometry (7). A repulsive interaction between Ser102 and phosphate is also suggested by recent analyses of structural and biochemical data for AP mutants at Ser102 and Arg166 (12). A repulsive interaction could contribute to the catalytic cycle or regulation of the enzyme by destabilizing the bound ground state and preventing saturation of the enzyme (13) and also by limiting inhibition of the enzyme by its phosphate product.

2. Comparisons to Prior Alkaline Phosphatase Structures

The structure reported here overlays closely with the previously reported structures of phosphate-bound AP, with alpha-carbon RMSD values of ~0.2 Å (Table S2).

The previously highest-resolution structure of phosphate-bound wild-type AP (1ED8, 1.75 Å) was reported with mixed occupancy of 60% Mg²⁺ and 40% Zn²⁺ in the magnesium-binding site (8). These occupancy values matched those of the modeled primary and secondary conformations of Ser102 in structure 1ED8, and thus it was suggested that the states were coupled and, further, that the catalytic role of Mg²⁺ was to facilitate deprotonation of Ser102 (8). Later studies provided strong evidence against this mechanistic interpretation, because an AP mutant incompatible with Mg²⁺ binding showed no change in catalytic activity towards phosphate diester hydrolysis, a reaction that is more sensitive to nucleophilic activation than is phosphate monoester hydrolysis (14).

In light of the apparently repulsive interaction between Ser102 and phosphate discussed in the prior section, the observations of different Ser102 occupancies in structures 1ED8 and 1ED9 suggest an interesting alternative interpretation. Prior structure 1ED9, which contains no bound phosphate, was refined with 100% occupancy of the primary ($\chi_1 = -60^\circ$) conformation of Ser102. In contrast, structure 1ED8, with full occupancy of phosphate, was refined with only 60% occupancy of the primary conformation of Ser102. The structure reported here had intermediate values in both cases, with phosphate and Ser102 occupancies of around 70% (see prior section). The structure reported herein was refined with 100% occupancy of the Mg²⁺ ion. Thus, when the new structure is considered, the serine occupancy appears coupled not to the Mg²⁺ occupancy, but instead to the phosphate occupancy. These observations are consistent with a repulsive interaction between Ser102 and phosphate, such that binding of phosphate leads to increased population of alternative Ser102 conformations.

An additional mechanistic interpretation from structure 1ED8 centered on anisotropic temperature factor refinement of the Arg166 sidechain. It was suggested that anisotropy of this sidechain correlated with a role in release and protonation of inorganic phosphate. While there is little doubt that Arg166 plays an important role in stabilizing the phosphoryl group in both the ground state and the transition state (10), refinement of the 1.29 Å structure provided no indication of notable anisotropy of the Arg166 sidechain.

Table S2. Available structures of wild-type *E. coli* alkaline phosphatase with bound phosphate

Structure	Resolution, Å	Space Group	Chain	Average B-Factor, Å ²	Residues	RMSD with current, Å ^a
Reported Herein	1.29 Å	P2 ₁	A	14.4	9-448	-
			B	13.9	9-448	
			C	16.2	9-448	
			D	15.1	6-448	
1ED8	1.75 Å	I ₂₂₂	A	22.4	1-449	0.24
			B	28.0	1-449	
1ALK	2.00 Å	I ₂₂₂	A	16.0	1-449	0.26
			B	22.1	1-449	

^a Alpha-carbon RMSD values between previously reported structures and the structure herein, averaged over the two dimers in the asymmetric unit.

3. Supporting Information for X-Ray Absorption Spectroscopy

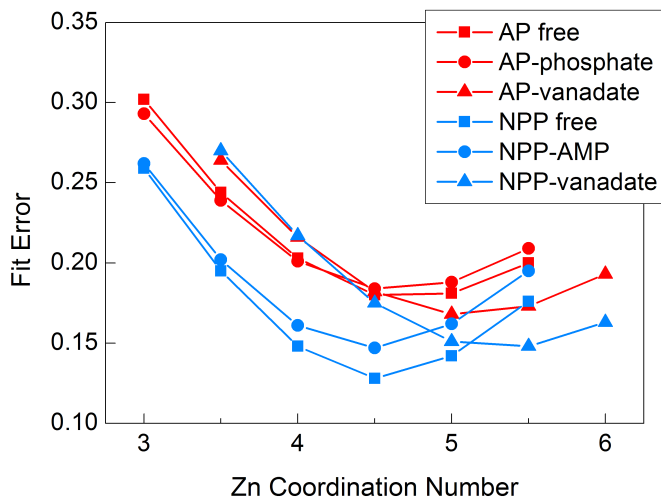


Figure S4. EXAFS fit error as a function of zinc coordination number for AP and NPP samples.

Table S3. First-shell EXAFS fitting results for AP and NPP samples for selected average zinc coordination numbers N .^a

Sample	Zn-N/O		
	R (Å)	N	$\sigma^2 \times 10^3$ (Å ²)
AP-free	1.98	4.0	5.6
	1.98	4.5	6.5
AP-phosphate	1.97	4.0	5.8
	1.97	4.5	6.8
	1.97	5.0	7.8
AP-vanadate	2.00	4.5	6.4
	2.00	5.0	7.3
	2.00	5.5	8.2
NPP-free	1.97	4.0	4.0
	1.97	4.5	4.9
NPP-AMP	1.97	4.0	4.0
	1.97	4.5	5.0
	1.97	5.0	5.8
NPP-vanadate	2.03	4.5	6.7
	2.03	5.0	7.8
	2.03	5.5	8.6

^a The estimated uncertainty in R is 0.02 Å.

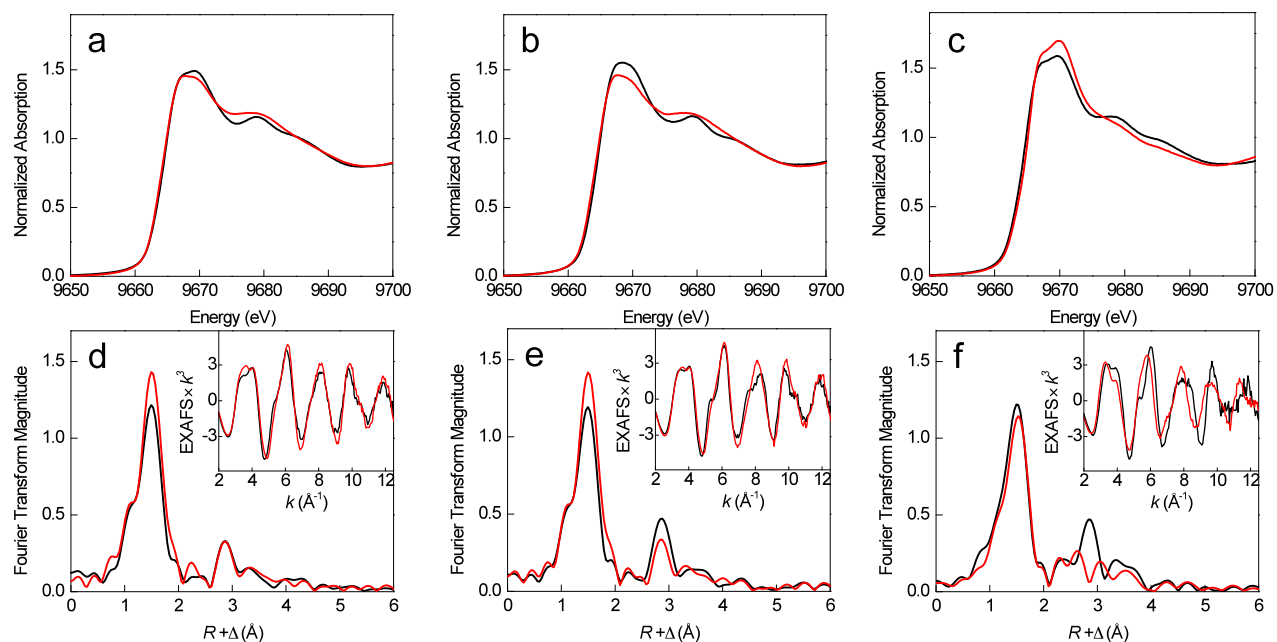


Figure S5. Overlay of the Zn K-edge XAS data for AP (black line) and NPP (red line) protein forms: (a-c) normalized edge spectra, and (d-f) nonphase-shifted Fourier transforms of the EXAFS data in insets. (a and d) Free enzyme forms (b and e) substrate analog-bound forms; AP bound to inorganic phosphate and NPP bound to AMP (c and f) AP and NPP bound to the vanadate transition state analog.

4. Comparison of Zn-ligand and Zn-Zn distances among available AP and NPP structures

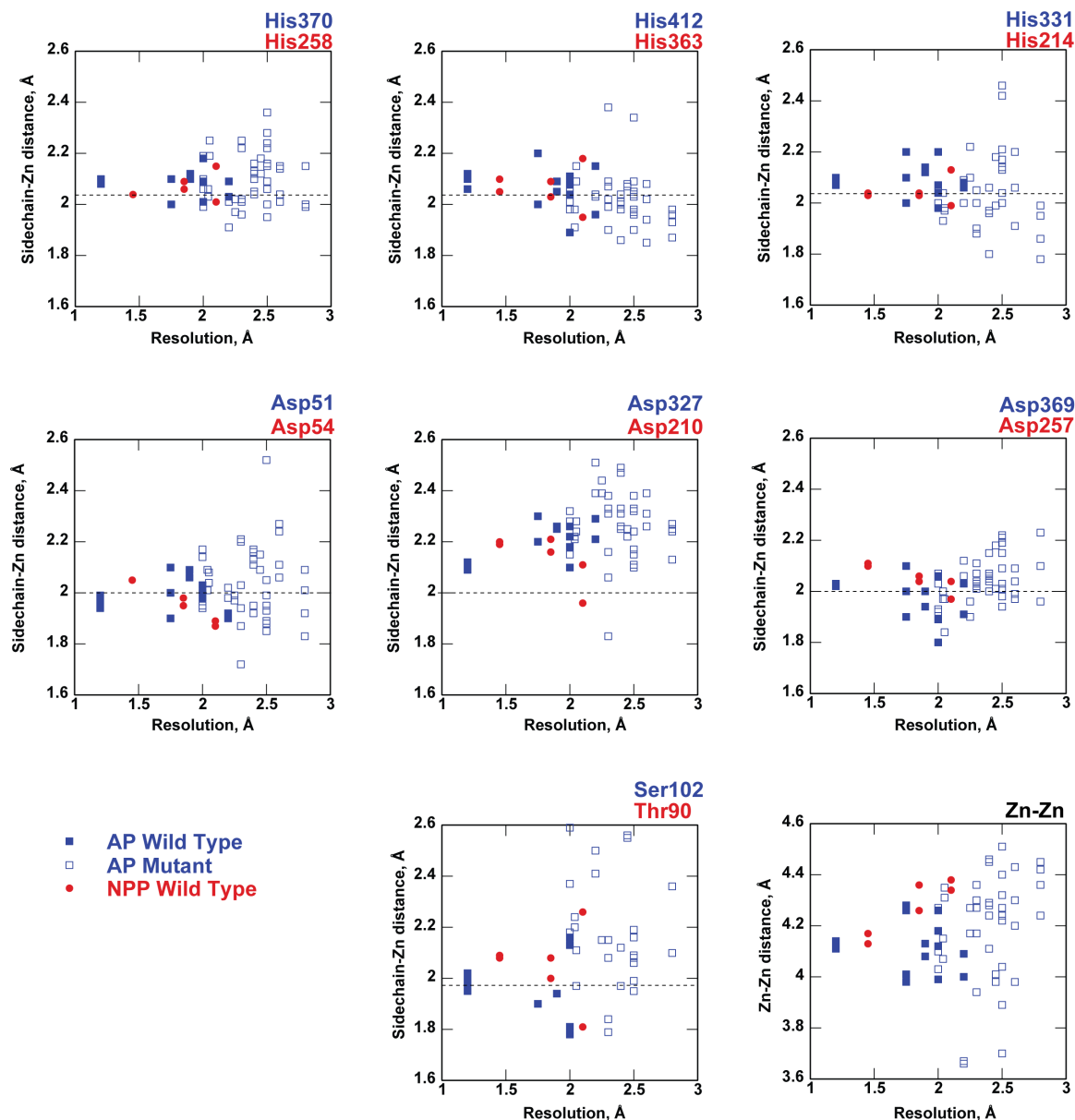


Figure S6. Comparison of Zn-ligand and Zn-Zn distances among the available structures of AP (blue) and NPP (red). Wild-type AP structures are shown in closed squares and mutants are shown in open squares. Both free enzymes and enzymes bound to substrate and transition state analogs are included in the plots. Each point represents a single active site within the asymmetric unit of the corresponding crystal structure. The dashed lines indicate average interaction distances from zinc-carboxylate and zinc-hydroxyl interactions from small-molecule crystal structures (15,16).

5. AP Preferentially Binds the Dianion Form of Vanadate (HVO_4^{2-})

The pH dependence of vanadate binding to *E. coli* AP was determined by following vanadate inhibition of the hydrolysis of *p*-nitrophenyl phosphorothioate (pNPPS). This substrate was used to avoid complications due to tight inhibition by the phosphate product released from reactions of phosphate monoester substrates. The pNPPS assay used here results in a slight underestimate of the affinity of vanadate for AP (see below), but it allowed measurements at low pH where signal can become limiting with low concentrations of phosphate ester substrates.

The pNPPS substrate was synthesized previously (17). Reactions were performed at 25 °C with 5-20 μM pNPPS, 0.015 μM enzyme, and 0.1-300 μM Na_3VO_4 in 1 M NaCl, 100 μM ZnCl_2 , 1 mM MgCl_2 , and 100 mM buffer. The buffers used were NaMES, pH 6.0; NaMalate, pH 6.5; NaMOPS, pH 7.0; Tris-Cl, pH 7.5; NaMOPS, pH 8.0; NaCHES, pH 8.5; and NaCHES, pH 9.0. Initial rates were determined and the dependence on vanadate concentration was fit with a binding equation. At all pH values, the substrate concentration was at least two-fold below the apparent K_M . Proximity to the K_M leads to error in the inhibition constant K_I (50% too high at pH 8), but this error does not affect the conclusions herein, which are based on 30-fold changes in K_I . The log of the association constant ($K_a = 1/K_I$) is plotted as a function of pH in Figure S7.

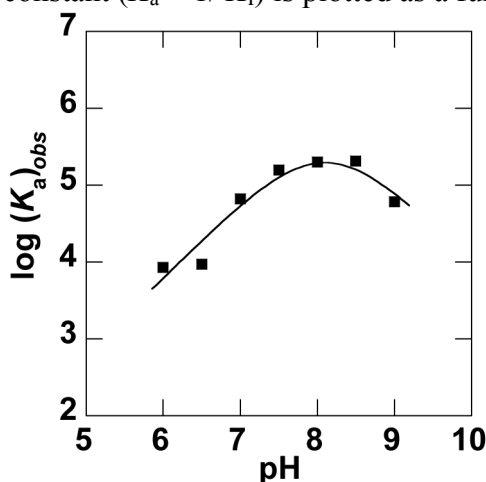


Figure S7. pH dependence of vanadate binding to AP, measured by inhibition of enzymatic hydrolysis of *p*-nitrophenyl phosphorothioate.

The pH-binding profile indicates the presence of two ionizations with similar pK_a values. The pK_a for ionization of vanadate monoanion ($\text{H}_2\text{VO}_4^{1-}$) to vanadate dianion (HVO_4^{2-}) is around 8, with values of 8.3 (18) and 7.8 (19) reported. Thus, the loss of affinity at lower pH values indicates that AP preferentially binds the vanadate dianion over the vanadate monoanion. The loss of affinity at $\text{pH} > 8$ is attributed to a previously described ionization of the free enzyme with a pK_a value of ~ 8.2 (20). The data were fit with the following relationship to reflect the two ionizations with similar pK_a values, resulting in a value of 8.1 for both pK_{a1} and pK_{a2} , and an upper limit for the dissociation constant of vanadate dianion of 1 μM .

$$\log(K_a)_{obs} = \log\left(\frac{K_a}{1 + 10^{pK_{a1} - pK_{a2}} + 10^{pK_{a1} - \text{pH}} + 10^{\text{pH} - pK_{a2}}}\right)$$

6. NPP Preferentially Binds the Monoanionic Forms of Vanadate and AMP

The pH dependence of NPP binding affinities for vanadate and AMP were measured by following the inhibition of enzyme activity with the substrate methyl *p*-nitrophenyl phosphate (MepNPP) under subsaturating conditions, as previously described (21). Reactions were performed at 25 °C, 0.1 M buffer, 0.5 M NaCl, 100 μM ZnCl₂, 100 μM MepNPP, 0.04 μM enzyme, and either 10 μM-100 mM Na₃VO₄ or 0.1 μM-10 mM AMP. Buffers used in these assays were NaMES, pH 6.0; NaMOPS, pH 7.0; Tris-Cl, pH 8.0; and NaCHES, pH 9.0. Initial rates were determined, plotted as a function of inhibitor concentration, and fit to a binding equation. The log of the association constant ($K_a = 1/K_i$) is plotted as a function of pH in Figure S8.

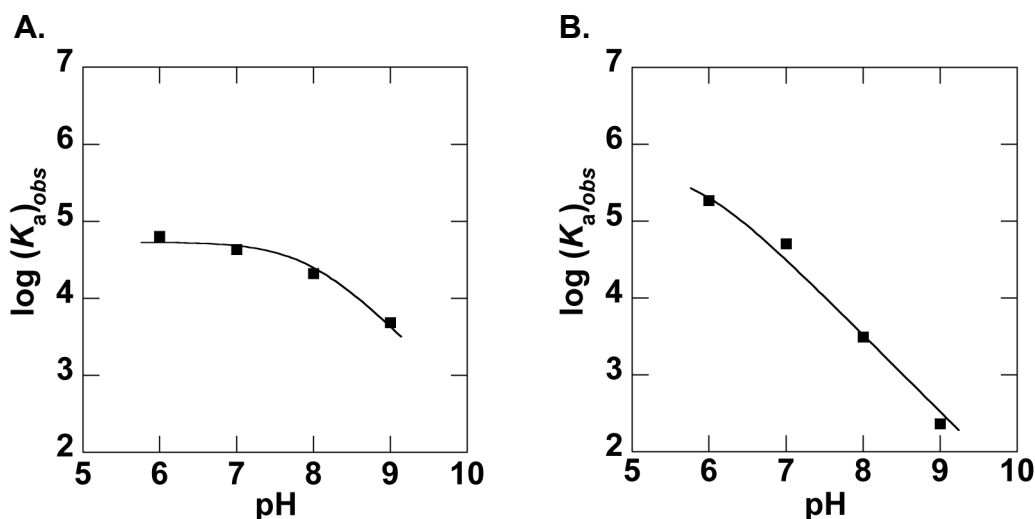


Figure S8. pH dependence of binding of vanadate (A) and AMP (B) to NPP, measured by inhibition of enzymatic hydrolysis of methyl *p*-nitrophenyl phosphate.

The reduction in binding affinity at high pH for both vanadate and AMP indicates that NPP preferentially binds the monoanionic forms of these inhibitors. The inhibition curves were fit with the following equation to account for a single pK_a . Best-fit values for vanadate were $pK_a = 7.9$ and $K_{i,low\ pH} = 19\ \mu\text{M}$. The fit of the data for AMP was consistent with reported pK_a values for AMP of 6.3 (22).

$$\log(K_a)_{obs} = \log\left(\frac{K_a}{1 + 10^{pH - pK_a}}\right)$$

References

1. Vanderkool, G. (1983) *J. Phys. Chem.* **87**, 5121-5129
2. Chakrabarti, P. (1993) *J. Mol. Biol.* **234**, 463-482
3. Jeffrey, G. A., and Maluszynska, H. (1982) *International Journal of Biological Macromolecules* **4**, 173-185
4. Wallwork, S. C. (1962) *Acta Cryst.* **15**, 758-759
5. McDonald, W. S., and Cruickshank, D. W. (1971) *Acta Cryst.* **B27**, 1315-1319
6. Olovsson, I., and Templeton, D. H. (1960) *Acta Chemica Scandinavica* **14**, 1325-1332
7. Steiner, T., and Saenger, W. (1994) *Acta Cryst.* **B50**, 348-357
8. Stec, B., Holtz, K. M., and Kantrowitz, E. R. (2000) *J. Mol. Biol.* **299**, 1303-1311
9. Adams, P. D., Grosse-Kunstleve, R. W., Hung, L. W., Ioerger, T. R., McCoy, A. J., Moriarty, N. W., Read, R. J., Sacchettini, J. C., Sauter, N. K., and Terwilliger, T. C. (2002) *Acta Cryst.* **D58**, 1948-1954
10. O'Brien, P. J., Lassila, J. K., Fenn, T. D., Zalatan, J. G., and Herschlag, D. (2008) *Biochemistry* **47**, 7663-7672
11. Allen, F. H. (2002) *Acta Cryst.* **B58**, 380-388
12. Andrews, L. D., and Herschlag, D. *Manuscript in preparation*
13. Andrews, L. D., Deng, H., and Herschlag, D. (2011) *J. Am. Chem. Soc.* **133**, 11621-11631
14. Zalatan, J. G., Fenn, T.D., Herschlag, D. (2008) *J. Mol. Biol.* **384**, 1174-1189
15. Harding, M. M. (2006) *Acta Cryst.* **D62**, 678-682
16. Kuppuraj, G., Dudev, M., and Lim, C. (2009) *J. Phys. Chem. B* **113**, 2952-2960
17. Hollfelder, F., and Herschlag, D. (1995) *Biochemistry* **34**, 12255-12264
18. Tracey, A. S., Jaswal, J. S., and Angus-Dunne, S. J. (1995) *Inorg. Chem.* **34**, 5680-5685
19. Crans, D. C., Smee, J. J., Gaidamauskas, E., and Yang, L. (2004) *Chem. Rev.* **104**, 849-902
20. O'Brien, P. J., and Herschlag, D. (2002) *Biochemistry* **41**, 3207-3225
21. Zalatan, J. G., Fenn, T. D., Brunger, A. T., and Herschlag, D. (2006) *Biochemistry* **45**, 9788-9803
22. Smith, R. M., and Alberty, R. A. (1956) *J. Phys. Chem.* **60**, 180-184